Theoretical analysis and simulation of phase separation in a driven bidirectional two-lane system

Qing-Yi Hao [1,2,*] Rui Jiang,[3] Mao-Bin Hu,[4] Yunxin Zhang,[2] Chao-Yun Wu,[1,4] and Ning Guo[5]

[1]*Key Laboratory of Modeling, Simulation and Control of Complex Ecosystem in Dabie Mountains of Anhui Higher Education Institutes,*
School of Mathematics and Computational Science, Anqing Normal University, Anqing 246133, China
[2]*School of Mathematical Sciences, Fudan University, Shanghai 200433, China*
[3]*MOE Key Laboratory for Urban Transportation Complex Systems Theory and Technology,*
Beijing Jiaotong University, Beijing 100044, China
[4]*School of Engineering Science, University of Science and Technology of China, Hefei 230026, China*
[5]*School of Automotive and Transportation Engineering, Hefei University of Technology, Hefei 230009, China*

The two-lane driven system is a type of important model to research some transport systems, and also a powerful tool to investigate properties of nonequilibrium state systems. This paper presents a driven bidirectional two-lane model. The dynamic characteristics of the model with periodic boundary are investigated by Monte Carlo simulation, simple mean field, and cluster mean field methods, respectively. By simulations, phase separations are observed in the system with some values of model parameters. When the phase separation does not occur, cluster mean field results are in good agreement with simulation results. According to the cluster mean field analysis and simulations, a conjecture about the condition that the phase separation happens is proposed. Based on the conjecture, the phase boundary distinguishing phase separation state and homogeneous state is determined, and a corresponding phase diagram is drawn. The conjecture is validated through observing directly the spatiotemporal diagram and investigating the coarsening process of the system by simulation, and a possible mechanism causing the phase separation is also discussed. These outcomes maybe contribute to understand deeply transport systems including the congestion and efficiency of the transport, and enrich explorations of nonequilibrium state systems.

I. INTRODUCTION

As the most prominent paradigm of the driven diffusive system, the asymmetric exclusion process (ASEP) is widely applied in various fields [1] since it was proposed originally by MacDonald and Gibbs in 1968 [2]. Specifically, various ASEP extended models are developed to model and analyze biological transport [1,3–8], vehicle traffic, and pedestrian traffic systems [9–12]. In addition to the practical application background, these transport systems can also be used as tools for the study of far from thermal equilibrium systems [13,14].

Most of these models are considered in single-channel systems [15–18], and there are also many of these models that are investigated in two-channel [19–21] or multiple-channel systems [22–25]. The two-channel system is a quasi-one-dimensional system involving just two "lanes", in which various rules are considered and some nonequilibrium properties are observed. In these two-channel models, some involve only one species of particles in systems. Particles move in each lane unidirectionally without lane change, but the movement of a particle in one of the lanes is affected by particles in another lane [26]; or unidirectional movements with lane change are considered [27–30]. Some of two-channel models focus on bidirectional movements with two species of particles in systems. One type of them takes into account that particles

move unidirectionally in each lane but opposite direction for two parallel lanes, in which there are interactions between particles on two lanes but no lane change [31]. Other models investigate that two species of particles move to opposite direction in each lane with a lane change [32,33]. Additional models consider the bottleneck effect, namely, a single lane is combined in the middle part of the two-channel system [34], and some models couple with the Langmuir kinetics [35]. These rules or considerations are mainly based on biological transport and traffic flow. In addition to simulating real transport rules and analyzing characteristics of the transport systems, many properties such as non-equilibrium systems have been found including phase transition [36,37], shock [38], phase separation [31,39], spontaneous symmetry breaking [21,40], the finite-size effect [33], and so on.

Though many ASEP models with two lanes have been investigated [31–35], various interactions based on real background of the transport systems such as molecular motors, pedestrians and vehicles have not been fully explored in two-channel systems, and more properties corresponding to non-equilibrium systems are to be studied further.

In this paper, inspired by vehicle or electric bicycle driving in opposite directions on a narrow road, a new bidirectional two-channel ASEP model is proposed. The interactions of particles between two lanes are considered in the model. Computer simulation and mean-field analysis are carried out to calculate the flow rate under periodic boundary conditions. Phase separation can be observed in the system for specific

_____
*haoqy@aqnu.edu.cn
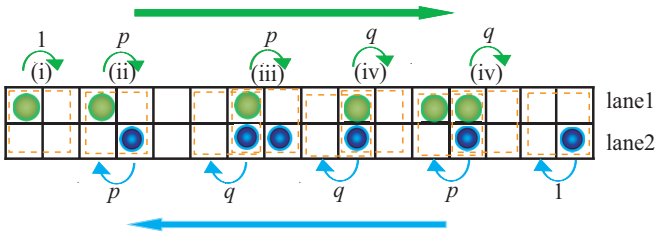
FIG. 1. Schematic illustration of the bidirectional two-lane TASEP model. Green full circle indicates the particle in upper lane (lane 1), blue full circle indicates the particle in lower lane (lane 2). The top and bottom boundaries are closed. The left and right boundaries are periodic. The arrows show moving direction of particles.

parameter values. When phase separation does not occur, the results from the two-vertical-horizontal-cluster mean-field method (CMF) are in good agreement with the results from computer simulation. A speculation under which conditions phase separation happens is given. Based on it, a phase boundary distinguishing phase separation state and homogeneous state is drawn, and the phase boundary is verified through investigating the coarsening process of the system by simulation.

The paper is organized as follows. The model is described in Sec. II. Simulation results and mean-field analysis are presented in Sec. III. Finally, conclusions are summarized in Sec. IV.

II. MODEL

A bidirectional two-lane model is presented as shown in Fig. 1. with two types of particles in the system: moving to the right and moving to the left. L sites are in each lane, and each site can only hold one particle. In lane 1, particles move from the left to the right, on the contrary, in lane 2, particles move from the right to the left. And change-lane behavior is not allowed in this two-lane system. When a site in lane 1 is selected randomly, if the site is occupied by a particle and the front neighboring site is empty, this two nearest-neighbor site pair is regarded as a bond; if the site selected is empty and the behind neighboring site is occupied by a particle, this two nearest-neighbor site pair is also regarded as a bond. For ease of expression, the site occupied by a particle in a bond is labeled i. If a bond in lane 1 is selected according to the random update rule, the movement of the particle in the bond is as follows:

(i) if the sites i and $i + 1$ in lane 2 are both empty, the particle in the bond will move to the front neighboring site $i + 1$ with rate 1 [see Fig. 1(i)].

(ii) if the site $i + 1$ is occupied in lane 2, the particle in the bond will move to the front neighboring site $i + 1$ with rate p [see Fig. 1(ii) and 1(iii)].

(iii) if the site i in lane 2 is occupied and the site $i + 1$ in lane 2 is empty, the particle in the bond will move to the front neighboring site $i + 1$ with rate q [see Fig. 1(iv)].

The movement rule of a particle in site i of lane 2 is similar to the above rule exchanging "lane 2" and "lane 1"

and changing "$i + 1$" to "$i - 1$". In case of $p = q = 1$, the model in each lane degenerates into the original TASEP model [15]. The background of this model rule can be from a vehicle or electric bicycle traffic. Considering safety and speed, on a narrow road, the driver in lane 1 may slow down in cases (ii) and (iii) as shown in Fig. 1, because the vehicle or electric bicycle in lane 1 will get into the front site side by side with a opposite vehicle or electric bicycle in lane 2. In case (iv), the driver in lane 1 will maybe move forward faster than in cases (ii) and (iii), because the vehicle or electric bicycle in lane 1 has kept side by side with an opposite vehicle or electric bicycle in lane 2, but there is no vehicle or electric bicycle in lane 2 in front of it. In case (i), the driver can move fast and freely, so the hopping rates are set to 1 for simplicity.

The periodic boundary condition is employed in the model, that is to say, the particles conservation system is considered. The density ρ defined as particle numbers in lane 1 divided by L is set to be equal to that of lane 2.

In this paper, we only study the case that the densities of two lanes are equal, i.e., $\rho_1 = \rho_2 = \rho$, which corresponds to the case of the balanced flow in pedestrian counterflow [41]. Here, ρ_1 and ρ_2 denote the density on lanes 1 and 2, respectively.

If considering this model from the thermodynamic view, the hopping rate p or q can be defined as $e^{\frac{E}{k_B T}}$, where E is the energy of an external field, k_B is the Boltzmann constant, and T is thermodynamic temperature [7,18,29]. It is assumed that particles move under short-range interaction which are driven by an external field with energy E ($E > 0$ indicates attraction interactions and $E < 0$ describes repulsion interactions). Creating [configuration (ii) in Fig. 1] and breaking configuration (iv) in Fig. 1] the pair of particles in one vertical cluster can be regarded as opposite chemical transitions. The system can be viewed as abiding detailed balance if $\frac{p}{q} = e^{\frac{E}{k_B T}}$ [7]. But the values of p and q are not limited by this relationship in the following discussions.

III. MEAN-FIELD ANALYSIS AND SIMULATION

The dynamical properties of the model are to be investigated by mean field analysis [9,26,31] and Monte Carlo simulations. The periodic boundary condition is employed in the model, that is to say, the particles conservation system is considered. The density ρ defined as particle numbers in lane 1 divided by L is set to be equal to that of lane 2.

A. Simple mean-field method

The mean field method has worked as a theoretical analysis tool for studying multi-body particle systems. Note that the mean field theory assumes that the particle system is always homogeneous at all densities. The simple mean field (SMF) that neglects all correlations between the state variables has the advantage of low computational cost, and works well in a system with very weak or no interactions [15,42]. Now, the current of the system is calculated by simple mean field method. For this purpose, the four probabilities corresponding to four vertical cluster configurations "0", "1", "2", "3" as shown in Fig. 2(a) are denoted as P_0, P_1, P_2, P_3, respectively. Ignoring correlations, the occupation of vertical clusters is
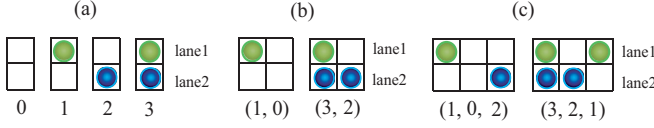
FIG. 2. Configurations of vertical clusters. (a) All four one-cell cluster configurations, (b) Two of all 16 two-cell cluster configurations, and (c) two of all 64 three-cell cluster configurations. The number labeled below vertical cluster indicates the type of the vertical cluster.

FIG. 3. Configurations schematics of three-cell cluster $(1,\underline{0},2)$ and $(\underline{3},\underline{2},1)$. The thick orange box indicates the target two-cell cluster to be considered.

assumed to be independent of the site in the lanes, i.e., $P(\tau, \gamma) = P_\tau \cdot P_\gamma$. Here, $\{\tau, \gamma\} \in \{0, 1, 2, 3\}$, and $P(\tau, \gamma)$ indicates the probability of two adjacent vertical clusters with configuration τ and γ.

From the definition of probability, one can get easily

$$P_0 + P_1 + P_2 + P_3 = 1. \tag{1}$$

The definition of density can indicate

$$P_1 + P_3 = \rho \tag{2}$$

and

$$P_2 + P_3 = \rho. \tag{3}$$

The master equations can describe the evolutions of the four probabilities. Especially, for P_1, the master equation is

$$\frac{dP_1}{dt} = 2P_3P_0q - 2P_1P_2p - P_3P_1p - P_1P_0, \tag{4}$$

when the system is in a steady state, $\frac{dP_1}{dt} = 0$. Thus,

$$pP_1P_2 = qP_0P_3. \tag{5}$$

Substituting Eqs. (1)–(3) into Eq. (5), we obtain

$$(q - p)P_1^2 - qP_1 + q(\rho - \rho^2) = 0. \tag{6}$$

Solving Eq. (6), we obtain the solution

$$P_1 = \begin{cases} \frac{q - \sqrt{q^2 + 4q(q-p)(\rho - \rho^2)^2}}{2(q-p)}, & p \neq q \\ \rho(1 - \rho), & p = q \end{cases}. \tag{7}$$

Substituting Eq. (7) into Eqs. (1)–(3), P_0, P_1, P_2 can be calculated, respectively. Thus, the currents on lanes 1 and 2 are

$$J_1 = P_1P_0 + P_1P_2p + P_3P_0q + P_3P_2p \tag{8}$$

and

$$J_2 = P_0P_2 + P_1P_2p + P_0P_3q + P_1P_3p. \tag{9}$$

From Eqs. (2) and (3), we have $P_1 = P_2$. So the currents on lanes 1 and 2 are equal, i.e., $J_1 = J_2$. When $p \neq q$, the expression of the current is

$$J = \frac{(p^2\rho + q\rho)(k + q - 2q\rho) - pk(q + \rho + q\rho - 1) - w}{2(p - q)^2}, \tag{10}$$

where

$$k = \sqrt{q(q(1 - 2\rho)^2 - 4p(-1 + \rho)\rho)} \tag{11}$$

and

$$w = pq(1 + \rho - 2\rho^2) + pq^2(1 - \rho + 2\rho^2). \tag{12}$$

When $p = q$, the expression of flow rate is

$$J = \rho + (2p - 3)\rho^2 + (3 - 3p)\rho^3 + (p - 1)\rho^4. \tag{13}$$

B. Cluster mean-field method

Next, the cluster mean field method, taking into account the correlation between particles, is employed to calculate the current of the system. $P(\sigma_1, \sigma_2, \ldots, \sigma_n)$ is used to denote the probability of finding an n-cell cluster in the state $(\sigma_1, \sigma_2, \ldots, \sigma_n)$ in the stationary state of the system. Here, the n-cell cluster is a collection of n successive vertical clusters. Considering that hop rates in the model depend on the states of two adjacent vertical clusters, we only involve a two-cell (two adjacent vertical clusters) cluster mean field analysis. In this case, the state of the two-cell cluster (σ_i, σ_{i+1}) as shown in Fig. 2(b) at time $t + 1$ depends on the state of the three-cell cluster $(\sigma_{i-1}, \sigma_i, \sigma_{i+1})$ or $(\sigma_i, \sigma_{i+1}, \sigma_{i+2})$ at time t as shown in Fig. 2(c) or Fig. 3. Here, the $\sigma_i = 0, 1, 2, 3$, corresponds to the four states shown in Fig. 2(a), respectively. Thus 16 two-cell cluster probabilities $P(\sigma_i, \sigma_{i+1})$ need to be solved.

Based on the model rules, the master equation of $P(1, 0)$ can be written as

$$\frac{dP(1, 0)}{dt} = P(1, 0) \mid_{\text{generation}} - P(1, 0) \mid_{\text{disappearance}}$$

$$= \left(\sum_{\tau \in \{1,3\}} P(\tau, \underline{0}, 0)q^{\frac{\tau-1}{2}} + \sum_{\tau \in \{0,1\}} P(\tau, \underline{3}, 0)(\tau p + (1 - \tau)q) \right.$$

$$\left. + \sum_{\tau \in \{0,2\}} P(\underline{1}, 1, \tau)p^{\frac{\tau}{2}} \right) - \left(P(1, 0) + \sum_{\tau \in \{2,3\}} P(\underline{1}, 0, \tau)q^{\tau-2} \right). \tag{14}$$

Here, a line is added under σ_i and σ_{i+1} to make a distinction between $(\sigma_{i-1}, \sigma_i, \sigma_{i+1})$ and $(\sigma_i, \sigma_{i+1}, \sigma_{i+2})$ (see Fig. 3). According to the general n-cell cluster approximation [9,26], $P(\sigma_{i-1}, \sigma_i, \sigma_{i+1})$ and $P(\sigma_i, \sigma_{i+1}, \sigma_{i+2})$ in the two-cell cluster mean field analysis can be expressed mathematically as

$$P(\sigma_{i-1}, \sigma_i, \sigma_{i+1}) = P(\sigma_{i-1}|\underline{\sigma_i})P(\sigma_i, \sigma_{i+1}) \tag{15}$$

and

$$P(\sigma_i, \sigma_{i+1}, \sigma_{i+2}) = P(\sigma_i, \sigma_{i+1})P(\underline{\sigma_{i+1}}|\sigma_{i+2}), \tag{16}$$

respectively, where

$$P(\sigma_{i-1}|\underline{\sigma_i}) = \frac{P(\sigma_{i-1}, \sigma_i)}{\sum_{\sigma_{i-1}} P(\sigma_{i-1}, \sigma_i)} \tag{17}$$

and

$$P(\underline{\sigma_{i+1}}|\sigma_{i+2}) = \frac{P(\sigma_{i+1}, \sigma_{i+2})}{\sum_{\sigma_{i+2}} P(\sigma_{i+1}, \sigma_{i+2})} \tag{18}$$

are two-cell cluster conditional probabilities. According to Eqs. (15) and (16), the three-cell cluster probabilities in the right-hand side of Eq. (14) can be converted to two-cell cluster probabilities. Noting $\frac{dP(1,0)}{dt} = 0$ when the system is in steady state, Eq. (14) can be simplified as

$$\frac{P(0,0) \sum_{\tau \in \{1,3\}} P(\tau,0)q^{\frac{\tau-1}{2}}}{\sum_{\tau \in \{0,1,2,3\}} P(\tau,0)} + \frac{P(3,0) \sum_{\tau \in \{0,1\}} P(\tau,3)(\tau p + (1-\tau)q)}{\sum_{\tau \in \{0,1,2,3\}} P(\tau,3)}$$
$$+ \frac{P(1,1) \sum_{\tau \in \{0,2\}} P(1,\tau)p^{\frac{\tau}{2}}}{\sum_{\tau \in \{0,1,2,3\}} P(1,\tau)} - \frac{P(1,0) \sum_{\tau \in \{2,3\}} P(0,\tau)q^{\tau-2}}{\sum_{\tau \in \{0,1,2,3\}} P(0,\tau)} - P(1,0) = 0 \ . \tag{19}$$

Due to the symmetry of the two lanes in the model, one can obtain the following six equations:

$$P(0,1) = P(2,0), \tag{20}$$

$$P(1,0) = P(0,2), \tag{21}$$

$$P(3,0) = P(0,3), \tag{22}$$

$$P(3,2) = P(1,3), \tag{23}$$

$$P(2,3) = P(3,1), \tag{24}$$

$$P(1,1) = P(2,2). \tag{25}$$

The conservation of probability requires that

$$\sum_{i,j=0}^{3} P(i,j) = 1. \tag{26}$$

Moreover, the definition of density indicates

$$\sum_{\tau \in \{0,1,2,3\}} \left(P(1,\tau) + P(3,\tau) \right) = \rho. \tag{27}$$

Another seven independent equations can be obtained similarly in the Appendix [Eqs. (A1)–(A7)]. Therefore, we have 16 equations including Eqs. (19)–(27) and (A1)–(A7) about 16 variables $P(\sigma_i, \sigma_{i+1})$. Obviously, the analytical solutions of the nonlinear equations cannot be obtained. So the Newton iteration method is used to compute the numerical solutions of the equations. Then the current of the system can be calculated as

$$J = P(1,0) + P(1,2)p + P(3,0)q + P(3,2)p \tag{28}$$

or

$$J = P(0,2) + P(1,2)p + P(0,3)q + P(1,3)p. \tag{29}$$

C. Simulations and discussions

Now we carry out the Monte Carlo simulations with $L = 2000$ and 10^6 Monte Carlo time steps (MCS). Particles move in each lane according to same model rule (see Fig. 1), just in the opposite direction. And simulation results show that the dynamical properties of the two lanes are the same. So only one lane of two lanes is represented in the following discussions, the quantitative or qualitative properties in the other lane is the same or similar.

The currents of the system with density $\rho \in [0, 1]$ for different values of parameters p and q are calculated by simulation, simple mean-field method (SMF), and cluster
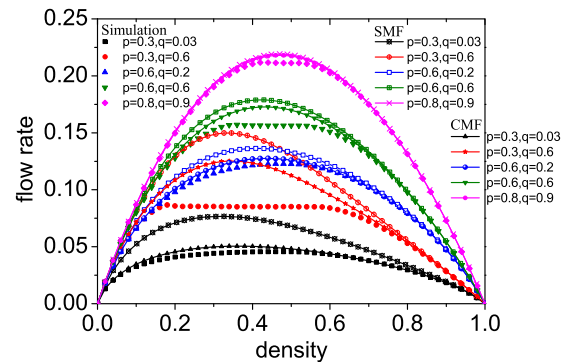
FIG. 4. Diagrams of current versus density ρ for five sets of different (p, q) values including $(p, q) = (0.3, 0.03)$, $(p, q) = (0.3, 0.6)$, $(p, q) = (0.6, 0.2)$, $(p, q) = (0.6, 0.6)$, and $(p, q) = (0.8, 0.9)$. The simulation results, simple mean-field results, and cluster mean-field results are compared together.
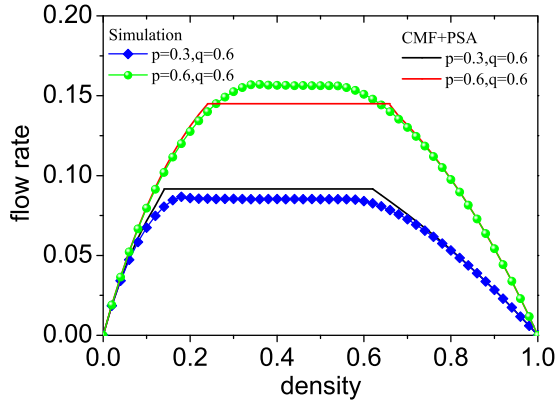
FIG. 5. Diagrams of current versus density from simulation and cluster mean-field analysis(CMF) combining phase separation approximation (PSA). For the CMF+PSA, the flow rate corresponding to the platform is calculated according to the CMF result at maximum point of $P(1, 2) + P(3, 2)$.

mean-field method (CMF), respectively. The corresponding plots are shown in Fig. 4. It can be seen that the current becomes large with the increase of p and q values. On the whole, the CMF result is better than the SMF result in agreement with the simulation result. However, it is easy to notice that the CMF result also deviates from the simulation result under some values of parameters p and q, such as $(p, q) = (0.3, 0.6)$, $(p, q) = (0.6, 0.6)$, $(p, q) = (0.8, 0.9)$. This is because the phase separation state occurs in the system,

which corresponds to the plateau in the flow rate curve as shown in Fig. 4. In this case, there are two critical densities ρ_{ca} and ρ_{cb}, which can also be observed clearly in Fig. 5. When $\rho < \rho_{ca}$, the flow rate increases with the increase of ρ; when $\rho > \rho_{cb}$, the flow rate decreases with the increase of ρ. In the intermediate density range $\rho_{ca} < \rho < \rho_{cb}$, the flow rate keeps invariant, which brings about a plateau in the curve. The typical spatiotemporal patterns of this phase separation state are shown in Fig. 6(a), (b), and (e). "Free flow" phase and "congested flow" phase coexist in the system, that is to say, the system is separated into a low density region and high density region. The density of the low density region equals to the first critical density ρ_{ca}, and the density of the high density region equals to the second critical density ρ_{cb}.

In order to explicate what causes the phase separation in this system, some investigations are carried out. Interestingly, by cluster mean-field analysis, we find a conclusion: when the maximum of $P(1, 2) + P(3, 2)$ is larger than that of $P(1, 0) + P(3, 0)$, the system can appear to have phase separation at medium density (around the maximum point of the flow rate from cluster mean field analysis). The simulation results validate this conclusion as shown in Table I.

The coarsening process of the system based on simulation is to be investigated to verify deeply the above conclusion and explore the mechanism causing phase separation. For this purpose, the normalized residence distribution of a cluster of s particles interconnected is defined and denoted as $p(s)$. In fact, the $p(s)$ can be understood as the probability that a selected random particle is in a cluster of size s [33]. In a homogeneous state, the mathematical expectation of cluster size s, $E(s) =$
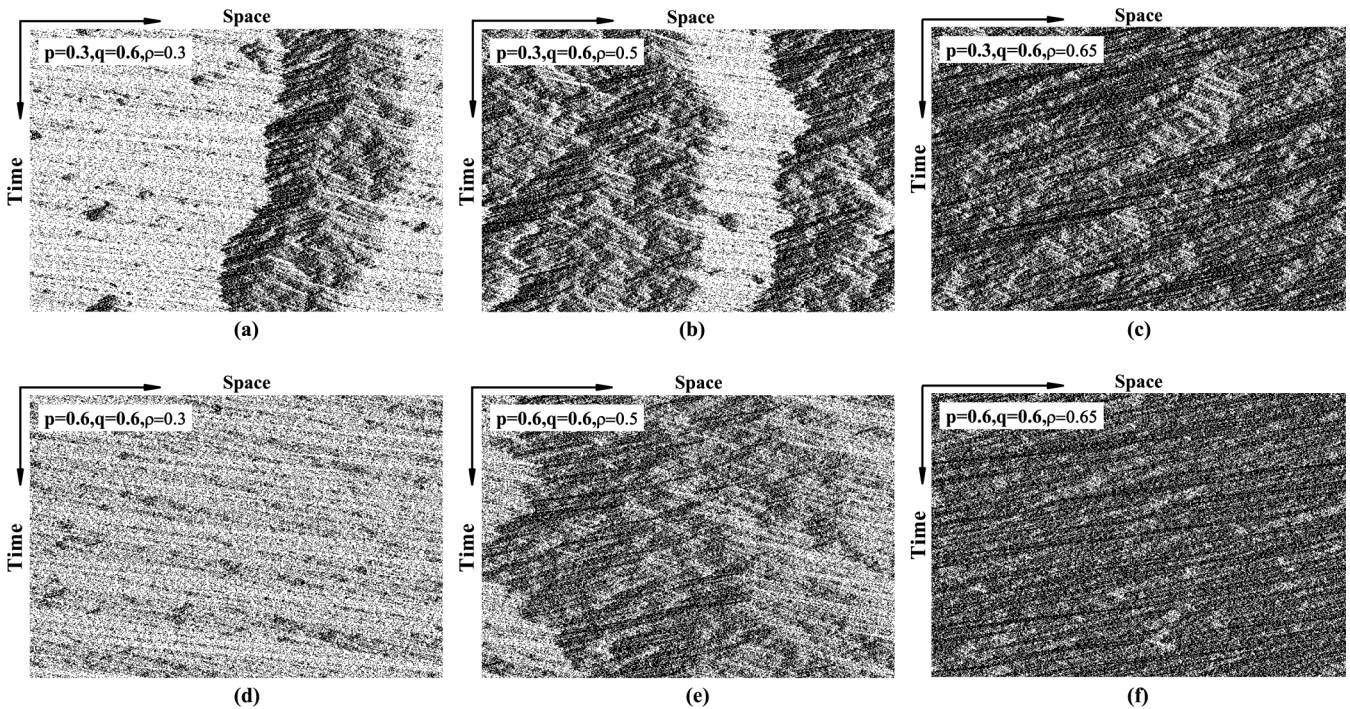
FIG. 6. Spatiotemporal diagram in one lane of two lanes. (a), (b), and (e) are phase separation states corresponding to the platform region; (c), (d), and (f) are macroscopic homogeneous states. The parameters are $p = 0.3$, $q = 0.6$, $\rho = 0.3$ in (a), $p = 0.3$, $q = 0.6$, $\rho = 0.5$ in (b), $p = 0.3$, $q = 0.6$, $\rho = 0.65$ in (c), $p = 0.6$, $q = 0.6$, $\rho = 0.3$ in (d), $p = 0.6$, $q = 0.6$, $\rho = 0.5$ in (e), and $p = 0.6$, $q = 0.6$, $\rho = 0.65$ in (f). 500 snapshots of the system are shown every 20 MC time steps after 5×10^4 time steps are discarded.

TABLE I. Maximum of $P(1,2) + P(1,3)$ and $P(1,0) + P(3,0)$ from CMF with different values of p and q.

(p, q)	Maximum of $P(1,2) + P(1,3)$	Maximum of $P(1,0) + P(3,0)$	Is phase separation?
$p = 0.3, q = 0.03$	0.085	0.179	No
$p = 0.3, q = 0.6$	0.177	0.109	Yes
$p = 0.6, q = 0.2$	0.117	0.160	No
$p = 0.6, q = 0.6$	0.153	0.137	Yes
$p = 0.8, q = 0.9$	0.154	0.141	Yes

$\sum_s s \cdot p(s)$ is small. Conversely, the mathematical expectation $E(s)$ is large in a phase separation state.

In (p, q) space, we can calculate the mathematical expectation $E(s)$ with given density ρ by simulation. For $\rho = 0.5$, the $E(s)$ in (p, q) space is shown in Fig. 7. One can note that the boundary line corresponding to $E(s) = 7$ is close to the boundary line corresponding to the maximum of $P(1,2) + P(3,2)$ being larger than that of $P(1,0) + P(3,0)$. This can also verify the above conclusion presented, when $E(s) > 7$, it indicates particles form some larger clusters, so the system appears at phase separation. Of course, the mean length of clusters $E(s) = 7$ is only approximate at the phase boundary. In fact, phase boundary should be in an interval.

Now we investigate $P(1,2) + P(3,2)$ and $P(1,0) + P(3,0)$. First, we focus on the case of the maximum of $P(1,2) + P(3,2)$ being larger than that of $P(1,0) + P(3,0)$. For $P(1,0) + P(3,0)$, it rises with the increase of density ρ. When $\rho = \rho_{ca}$, the value of $P(1,0) + P(3,0)$ reaches the maximum. Then the system transitions into phase separation, in which the value of $P(1,0) + P(3,0)$ maintains the maximum in the low density region. When $\rho > \rho_{cb}$, the system turns into homogeneous again, and the value of $P(1,0) + P(3,0)$ continues to decrease with the increase of ρ. When $\rho \in [\rho_{ca}, \rho_{cb}]$, the system is separated into a low density

region with $\rho = \rho_{ca}$ and a high density region with $\rho = \rho_{cb}$. With the increase of ρ, the low density region shrinks and the high density region expands. As a result, the mean value of $P(1,0) + P(3,0)$ decreases linearly with the increase of ρ due to $P(1,0) + P(3,0)$ maintaining the maximum value in the low density region and taking a small value in the high density region, as shown in Fig. 8(a). On the contrary, for $P(1,2) + P(3,2)$, it rises with the decrease of density from $\rho = 1$. When $\rho = \rho_{cb}$, the value of $P(1,2) + P(3,2)$ reaches the maximum. After that the phase separation emerges in the system. In this state, the value of $P(1,2) + P(3,2)$ holds the maximum in the high density region. When $\rho < \rho_{ca}$, the system returns to the homogeneous state, and the value of $P(1,2) + P(3,2)$ continues to decrease with the decrease of ρ. Similarly, in $\rho \in [\rho_{ca}, \rho_{cb}]$, the mean value of $P(1,2) + P(3,2)$ decreases linearly with the decrease of ρ due to $P(1,2) + P(3,2)$ holding the maximum value in the high density region and taking a small value in the low density region, as shown in Fig. 8(b). Based on these results and cluster mean field results, the flow rate corresponding to the plateau can be calculated approximately according to the CMF result at a maximum point of $P(1,2) + P(3,2)$ (see Fig. 5). Next, we discuss the case of the maximum of $P(1,2) + P(3,2)$ being less than that of $P(1,0) + P(3,0)$. In this case, it is inferred that the system cannot satisfy synchronously $P(1,2) + P(3,2)$ and $P(1,0) + P(3,0)$ to keep their maximum at any density. That is to say, for a given arbitrary ρ, the system cannot be divided spontaneously into a low density region in which $P(1,0) + P(3,0)$ maintains the maximum and a high density region in which $P(1,2) + P(3,2)$ keeps the maximum. Therefore, the system does not appear phase separated in this case.

According to the above investigation, one can argue that the phase separation is as a result of the system always trying to maximize $P(1,2) + P(3,2)$ and $P(1,0) + P(3,0)$ in the whole system and if not possible, in part of the system. Moreover, the range of the density at which the phase separation occurs can be calculated approximately according to the CMF result, that is from ρ_{ca} to ρ_{cb}. Here, ρ_{ca} is the maximum point of $P(1,0) + P(3,0)$ from CMF and ρ_{cb} is the maximum point of $P(1,2) + P(3,2)$ from CMF. By simulations, one can note that, when the value of q is fixed, the range of the density corresponding to the phase separation becomes narrow with the increase of p, but when the value of p is fixed, the range of the density corresponding to the phase separation does not nearly change (see Fig. 9). About the mechanism causing the phase separation, we guess that the phase separation is driven by the entropy of the system from thermodynamic viewpoints. According to different configurations of the two-cell vertical cluster, the system has similarly the so-called
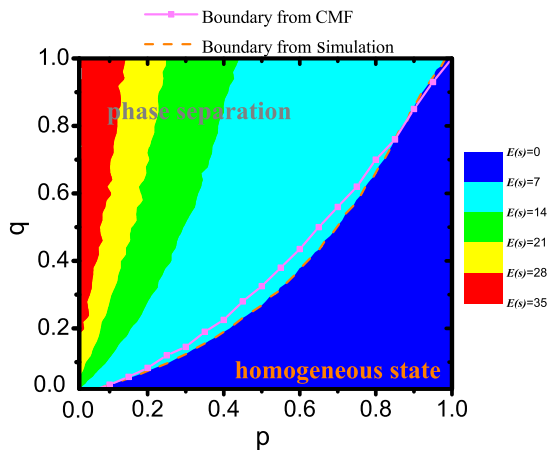
FIG. 7. Phase diagram. Boundary separating phase separation from homogeneous state in (p, q) space. The boundary lines are obtained from CMF with the relation $\max(P(1,2) + P(3,2)) > \max(P(1,0) + P(3,0))$, from a simulation with $\rho = 0.5$, respectively. Here, the different colors denote different mathematical expectation of cluster size $E(s)$, i.e., the mean length of clusters. The boundary from simulation is corresponding to the mean length $E(s) = 7$ of a cluster.
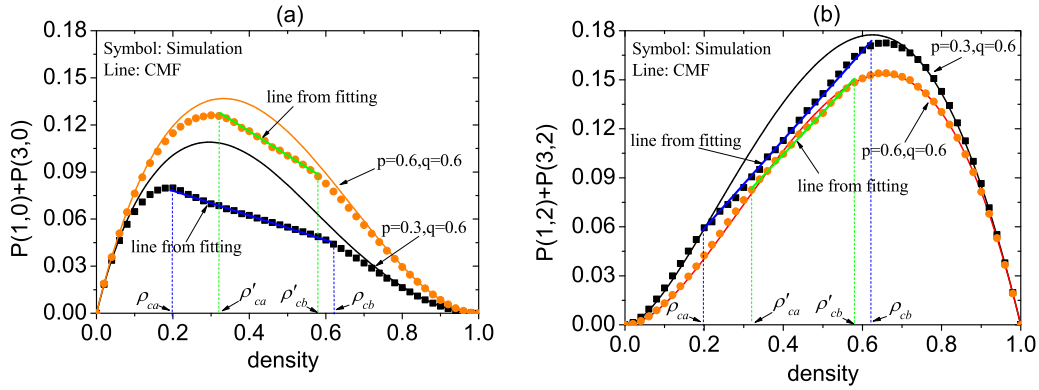
FIG. 8. Plots of (a) $P(1, 0) + P(3, 0)$ and (b) $P(1, 2) + P(3, 2)$ versus density from simulation and cluster mean-field analysis with $p = 0.3$, $q = 0.6$ and $p = 0.6$, $q = 0.6$. The dashed line is a guide for the eyes to see critical density value entering the phase separation state.

configuration entropy [43]. The entropy production leads to the phase separation. Presently we could only provide the possible and crude explanation about the mechanism, and the exact or clear mechanism of the phase separation is needed to explore under further investigations.

In real traffic systems [41,44], this phase separation phenomenon does exist, which corresponds to the "free flow" and "congested flow", or "synchronized flow" and "wide-moving jams" [45]. If the hopping rate p and q can be adjusted or induced to be in a certain range, the phase separation does not occur, and the real traffic system can only be in "free flow" or "synchronized flow" to improve the traffic efficiency.

Various traffic systems and related self-driven many-particle systems have been concerned [9,10]. Especially, the phase behavior or phase separation in a driven two-lane system has always been focused on. The nucleation or phase separation process was investigated in the two-lane system with two species of particles driven in opposite directions [33]. A possible phase separation mechanism was proposed in a bidirectional two-lane asymmetric exclusion process [31]. The steady-state phase diagrams for symmetrically split interaction strength were given in an open two-lane symmetrically coupled interacting TASEP model [29]. In addition, the phase

separation driven by the entropy has attracted the interest of researchers in related fields [46,47]. Our research may provide some new perspectives for these theoretical and applied fields.

IV. CONCLUSION

To summarize, this paper has presented a driven bidirectional two-lane model. Monte Carlo simulation, simple mean field and cluster mean field methods are employed, respectively, to research dynamic characteristics of the model with periodic boundary. By simulations, phase separations are observed in the system with some values of parameters (p, q). When the system does not occur phase separation, cluster mean field results are in good agreement with simulation results. Based on cluster mean field analysis and simulations, an inference is given that the system can appear at phase separation when the maximum of $P(1, 2) + P(3, 2)$ is larger than that of $P(1, 0) + P(3, 0)$. The phase diagram including phase separation state and homogeneous state is drawn, and the phase boundary from the above inference is validated through an investigation of the coarsening process of the system based on simulation. Possible mechanism about the phase separation is also discussed.
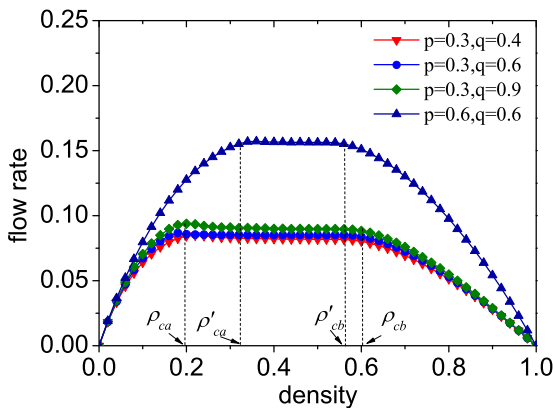
FIG. 9. Diagrams of current versus density by simulations with $p = 0.3$, $q = 0.4$; $p = 0.3$, $q = 0.6$; $p = 0.3$, $q = 0.9$; and $p = 0.6$, $q = 0.6$. The dashed line is a guide for the eyes to see critical density values ρ_{ca}, ρ_{cb}, ρ'_{ca}, ρ'_{cb} entering the phase separation state.

APPENDIX

In this Appendix, the other seven independent master equations for two-cell cluster probabilities are presented ignoring the derivation process, because the derivation method is similar to that of Eq. (19).

Analyzing the temporal evolution of two-cell cluster probability $P(0, 0)$ and $\frac{dP(0,0)}{dt} = 0$, we can get

$$
\frac{P(0, 1) \sum_{\tau \in \{0,2\}} P(1, \tau) p^{\frac{\tau}{2}}}{\sum_{\tau \in \{0,1,2,3\}} P(1, \tau)} + \frac{P(0, 2)P(2, 0)}{\sum_{\tau \in \{0,1,2,3\}} P(\tau, 2)} + \frac{P(1, 2)P(2, 0)p}{\sum_{\tau \in \{0,1,2,3\}} P(2, \tau)}
$$
$$
- \frac{P(0, 0) \sum_{\tau \in \{1,3\}} P(\tau, 0) q^{\frac{\tau-1}{2}}}{\sum_{\tau \in \{0,1,2,3\}} P(\tau, 0)} - \frac{P(0, 0) \sum_{\tau \in \{2,3\}} P(0, \tau) q^{\tau-2}}{\sum_{\tau \in \{0,1,2,3\}} P(0, \tau)} = 0 . \tag{A1}
$$

Considering the temporal evolution of $P(1, 1)$ and $\frac{dP(1,1)}{dt} = 0$, we can have

$$
\frac{P(0, 1) \sum_{\tau \in \{1,3\}} P(\tau, 0) q^{\frac{\tau-1}{2}}}{\sum_{\tau \in \{0,1,2,3\}} P(\tau, 0)} + \frac{P(3, 1) \sum_{\tau \in \{0,1\}} P(\tau, 3)(\tau p + (1 - \tau)q)}{\sum_{\tau \in \{0,1,2,3\}} P(\tau, 3)} - \frac{P(1, 1) \left(\sum_{\tau \in \{0,2\}} P(1, \tau) p^{\frac{\tau}{2}} + \sum_{\tau \in \{2,3\}} P(1, \tau) p \right)}{\sum_{\tau \in \{0,1,2,3\}} P(1, \tau)} = 0 . \tag{A2}
$$

Considering the temporal evolution of $P(3, 0)$ and $\frac{dP(3,0)}{dt} = 0$, we can obtain

$$
P(1, 2)p + \frac{P(2, 0) \sum_{\tau \in \{1,3\}} P(\tau, 2) p}{\sum_{\tau \in \{0,1,2,3\}} P(\tau, 2)} + \frac{P(3, 1) \sum_{\tau \in \{0,2\}} P(1, \tau) p^{\frac{\tau}{2}}}{\sum_{\tau \in \{0,1,2,3\}} P(1, \tau)} - P(3, 0)q
$$
$$
- \frac{P(3, 0) \sum_{\tau \in \{0,1\}} P(\tau, 3)(\tau p + (1 - \tau)q)}{\sum_{\tau \in \{0,1,2,3\}} P(\tau, 3)} - \frac{P(3, 0) \sum_{\tau \in \{2,3\}} P(0, \tau) q^{\tau-2}}{\sum_{\tau \in \{0,1,2,3\}} P(0, \tau)} = 0 . \tag{A3}
$$

Noting the temporal evolution of $P(1, 2)$ and $\frac{dP(1,2)}{dt} = 0$, we can have

$$
\frac{P(0, 2) \sum_{\tau \in \{1,3\}} P(\tau, 0) q^{\frac{\tau-1}{2}}}{\sum_{\tau \in \{0,1,2,3\}} P(\tau, 0)} + \frac{P(1, 0) \sum_{\tau \in \{2,3\}} P(0, \tau) q^{\tau-2}}{\sum_{\tau \in \{0,1,2,3\}} P(0, \tau)} + \frac{P(1, 3) \sum_{\tau \in \{0,2\}} P(3, \tau)(\frac{\tau}{2} p + (1 - \frac{\tau}{2})q)}{\sum_{\tau \in \{0,1,2,3\}} P(3, \tau)}
$$
$$
+ \frac{P(3, 2) \sum_{\tau \in \{0,1\}} P(\tau, 3)(\tau p + (1 - \tau)q)}{\sum_{\tau \in \{0,1,2,3\}} P(\tau, 3)} - 2P(1, 2)p = 0 . \tag{A4}
$$

Considering the temporal evolution of $P(2, 1)$ and $\frac{dP(2,1)}{dt} = 0$, we can obtain

$$
(P(3, 0) + P(0, 3))q - \frac{P(2, 1) \left(\sum_{\tau \in \{0,1\}} P(\tau, 2) p^{\tau} + \sum_{\tau \in \{1,3\}} P(\tau, 2) p \right)}{\sum_{\tau \in \{0,1,2,3\}} P(\tau, 2)} - \frac{P(2, 1) \left(\sum_{\tau \in \{0,2\}} P(1, \tau) p^{\frac{\tau}{2}} + \sum_{\tau \in \{2,3\}} P(1, \tau) p \right)}{\sum_{\tau \in \{0,1,2,3\}} P(1, \tau)} = 0 . \tag{A5}
$$

Analyzing the temporal evolution of $P(3, 1)$ and $\frac{dP(3,1)}{dt} = 0$, we can get

$$
P(1, 3)p + \frac{P(2, 1) \sum_{\tau \in \{1,3\}} P(\tau, 2) p}{\sum_{\tau \in \{0,1,2,3\}} P(\tau, 2)} - \frac{P(3, 1) \sum_{\tau \in \{0,1\}} P(\tau, 3)(\tau p + (1 - \tau)q)}{\sum_{\tau \in \{0,1,2,3\}} P(\tau, 3)}
$$
$$
- \frac{P(3, 1) \left(\sum_{\tau \in \{0,2\}} P(1, \tau) p^{\frac{\tau}{2}} + \sum_{\tau \in \{2,3\}} P(1, \tau) p \right)}{\sum_{\tau \in \{0,1,2,3\}} P(1, \tau)} = 0 . \tag{A6}
$$

Considering the temporal evolution of $P(3, 3)$ and $\frac{dP(3,3)}{dt} = 0$, we can have

$$\frac{P(2, 3) \sum\limits_{\tau \in \{1,3\}} P(\tau, 2)p}{\sum\limits_{\tau \in \{0,1,2,3\}} P(\tau, 2)} + \frac{P(3, 1) \sum\limits_{\tau \in \{2,3\}} P(1, \tau)p}{\sum\limits_{\tau \in \{0,1,2,3\}} P(1, \tau)}$$

$$- \frac{P(3, 3) \sum\limits_{\tau \in \{0,2\}} P(3, \tau)\left(\frac{\tau}{2}p + (1 - \frac{\tau}{2})q\right)}{\sum\limits_{\tau \in \{0,1,2,3\}} P(3, \tau)} - \frac{P(3, 3) \sum\limits_{\tau \in \{0,1\}} P(\tau, 3)(\tau p + (1 - \tau)q)}{\sum\limits_{\tau \in \{0,1,2,3\}} P(\tau, 3)} = 0. \quad \text{(A7)}$$

[1] T. Chou, K. Mallick, and R. K. P. Zia, Rep. Prog. Phys. **74**, 116601 (2011).

[2] C. T. Macdonald, J. H. Gibbs, and A. C. Pipkin, Biopolymers **6**, 1 (1968).

[3] N. Hirokawa, Science **279**, 519 (1998).

[4] I. Neri, N. Kern, and A. Parmeggiani, Phys. Rev. Lett. **110**, 098102 (2013).

[5] B. Mishra and D. Chowdhury, Phys. Rev. E **95**, 062117 (2017).

[6] S. Ghosh, B. Mishra, S. Patra, A. Schadschneider, and D. Chowdhury, J. Stat. Mech. (2018) 043203.

[7] H. Teimouri, A. B. Kolomeisky, and K. Mehrabiani, J. Phys. A: Math. Theor. **48**, 065001 (2015).

[8] I. Pinkoviezky and N. S. Gov, New J. Phys. **15**, 025009 (2013).

[9] D. Chowdhury, L. Santen, and A. Schadschneider, Phys. Rep. **329**, 199 (2000).

[10] D. Helbing, Rev. Mod. Phys. **73**, 1067 (2000).

[11] T. Wang, J. Zhang, Z. Y. Gao, W. Y. Zhang, and S. B. Li, Nonlinear Dyn. **88**, 1345 (2017).

[12] G. H. Peng, S. H. Yang, D. X. Xia, and X. Q. Li, Nonlinear Dyn. **94**, 2969 (2018).

[13] G. M. Schütz, Integrable Stochastic Many-Body Systems, in *Phase Transitions and Critical Phenomena*, edited by C. Domb and J. L. Lebowitz (Academic Press, London, 2001), Vol. 19, p. 1C251.

[14] M. Z. Liu, S. D. Li, and R. L. Wang, Chin. Phys. B **21**, 090510 (2012).

[15] B. Derrida, Phys. Rep. **301**, 65 (1998).

[16] S. Klumpp and R. Lipowsky, Europhys. Lett. **66**, 90 (2004).

[17] D. Celis-Garza, H. Teimouri, and A. B. Kolomeisky, J. Stat. Mech. (2015) P04013.

[18] Q. Y. Hao, Z. Chen, X. Y. Sun, B. B. Liu, and C. Y. Wu, Phys. Rev. E **94**, 022113 (2016).

[19] V. Popkov and I. Peschel, Phys. Rev. E **64**, 026126 (2001).

[20] A. Melbinger, T. Reichenbach, T. Franosch, and E. Frey, Phys. Rev. E **83**, 031923 (2011).

[21] E. Pronina, A. B. Kolomeisky, J. Phys. A **40**, 2275 (2007).

[22] A. K. Verma, A. K. Gupta, and I. Dhiman, Europhys. Lett. **112**, 30008 (2015).

[23] I. Dhiman and A. K. Gupta, Phys. Lett. A **380**, 2038 (2016).

[24] Z. P. Cai, Y. M. Yuan, R. Jiang, M. B. Hu, Q. S. Wu, and Y. H. Wu, J. Stat. Mech. (2008) P07016.

[25] Y. Q. Wang, B. Jia, R. Jiang, Z. Y. Gao, W. H. Li, K. J. Bao, and X. Z. Zheng, Nonlinear Dyn. **88**, 1 (2017).

[26] Q. Y. Hao, R. Jiang, C. Y. Wu, N. Guo, B. B. Liu, and Y. X. Zhang, Phys. Rev. E **98**, 062111 (2018).

[27] M. Kanai, Phys. Rev. E **82**, 066107 (2010).

[28] I. Dhiman and A. K. Gupta, Int. J. Mod. Phys. C **29**, 1850037 (2018).

[29] T. Midha, A. K. Gupta, and A. B. Kolomeisky, J. Stat. Mech. (2017) 073202.

[30] Z. J. Ding, T. Liu, X. X. Lou, Z. W. Shen, K. J. Zhu, R. Jiang, B. H. Wang, and B. K. Chen, Physica A **516**, 317 (2019).

[31] R. Jiang, K. Nishinari, M. B. Hu, Y. H. Wu, and Q. S. Wu, J. Stat. Phys. **136**, 73 (2009).

[32] J. T. Mettetal, B. Schmittmann, and R. K. P. Zia, Europhys. Lett. **58**, 653 (2002).

[33] I. T. Georgiev, B. Schmittmann, and R. K. P. Zia, Phys. Rev. Lett. **94**, 115701 (2005).

[34] V. Popkov, M. R. Evans, and D. Mukamel, J. Phys. A **41**, 1626 (2008).

[35] N. Sharma and A. K. Gupta, J. Stat. Mech. (2017) 043211.

[36] A. Nagar, M. Ha, and H. Park, Phys. Rev. E **77**, 061118 (2008).

[37] Y. Q. Wang, R. Jiang, A. B. Kolomeisky, and M. B. Hu, Sci. Rep. **4**, 5459 (2014).

[38] K. Nishinari, Y. Okada, A. Schadschneider, and D. Chowdhury, Phys. Rev. Lett. **95**, 118101 (2005).

[39] Y. Kafri, E. Levine, D. Mukamel, G. M. Schütz, and R. D. Willmann, Phys. Rev. E **68**, 035101(R) (2003).

[40] M. R. Evans, D. P. Foster, C. Godreche, and D. Mukamel, Phys. Rev. Lett. **74**, 208 (1995).

[41] V. J. Blue and J. L. Adler, Transp. Res. Part B **35**, 293 (2001).

[42] Q. Y. Hao, R. Jiang, M. B. Hu, and Q. S. Wu, Phys. Rev. E **82**, 022103 (2010).

[43] A. Takada, R. Conradt, and P. Richet, Entropy **20**, 218 (2018).

[44] B. S. Kerner, Phys. Rev. E **65**, 046138 (2002).

[45] Y. M. Yuan, R. Jiang, Q. S. Wu, and R. Wang, Int. J. Mod. Phys. C **18**, 267 (2007).

[46] R. P. Sear, Phys. Rev. E **56**, 4463 (1997).

[47] Y. D. Zhang, A. G. Xu, G. C. Zhang, Y. B. Gan, Z. H. Chen, and S. Succi, Soft Matter **15**, 2245 (2019).